

Study of Atrial Arrhythmias in a Computer Model Based on MR Images of Human Atria

N. Virag,^{a,c} V. Jacquemet,^a C. S. Henriquez,^{b,d}
S. Zozor,^a O. Blanc,^a J.-M. Vesin,^a
E. Pruvot,^b L. Kappenberger^b

^a *Signal Processing Institute, EPFL, CH-1015 Lausanne, Switzerland*

^b *Division of Cardiology, CHUV, CH-1011 Lausanne, Switzerland*

^c *Medtronic Europe SA, CH-1131 Tolothenaz, Switzerland*

^d *Department of Biomedical Engineering, Duke University,
Durham, NC 27708-0281 USA*

Published in Chaos (2002), vol. 12, no. 3, pp. 754-763

Abstract

The maintenance of multiple wavelets appears to be a consistent feature of atrial fibrillation (AF). In this paper, we investigate possible mechanisms of initiation and perpetuation of multiple wavelets in a computer model of AF. We developed a simplified model of human atria that uses an ionic-based membrane model and whose geometry is derived from a segmented MRI dataset. The three-dimensional surface has a realistic size and includes obstacles corresponding to the location of major vessels and valves, but it does not take into account anisotropy. The main advantage of this approach is its ability to simulate long duration arrhythmias (up to 40 seconds). Clinically relevant initiation protocols, such as single-site burst pacing, were used. The dynamics of simulated AF were investigated in models with different action potential durations and restitution properties, controlled by the conductance of the slow inward current in a modified Luo-Rudy model. The simulation studies show that (1) single-site burst pacing protocol can be used to induce wavebreaks even in tissue with uniform membrane properties, (2) the restitution-based wavebreaks in an atrial model with realistic size and conduction velocities are transient and (3) a significant reduction in APD (even with apparently flat restitution) increases the duration of AF.

Atrial arrhythmias are the most frequent rhythm disorder in humans and often lead to severe complications such as heart failure and stroke. While different mapping techniques have provided significant information on the electrophysiological processes associated with atrial fibrillation (AF), the mechanisms underlying its initiation and maintenance remain unclear. Hence the treatment of atrial arrhythmias is still based on empirical considerations. To assist the study of the complex, spatio-temporal dynamics of AF, we developed a realistic-size computer model of human atria. The model geometry is derived from MRI images of the human heart. By representing the domain as a three-dimensional monolayer, the computational load is sufficiently reduced to allow the simulation of up to 40 seconds of an arrhythmia. With this model, simulated atrial fibrillation (SAF), i.e. multiple reentrant wavelets, can be induced using a single-site burst pacing protocol. The model outputs both transmembrane potential maps and electrograms at any location in the atria, facilitating comparisons of simulation results to experimental or clinical data. Using the model, it is possible to study separately the parameters leading to the initiation of and perpetuation of AF. The simulation studies suggest that the restitution dynamics (describing the dependence of the action potential duration on the previous diastolic interval) and the action potential duration may play a crucial role in determining the duration of AF.

1 Introduction

Different mapping techniques have provided experimental clues on the relevant electrophysiological processes initiating or sustaining arrhythmia. Experimental models of atrial fibrillation (AF) usually involve an intervention, such as the application of a drug or chronic pacing [1, 2, 3, 4] to create a substrate for arrhythmogenesis. Often interventions cause considerable shortening of both the effective refractory period and spatial wavelengths, increasing the likelihood of arrhythmias. The maintenance of multiple wavelets appears to be a consistent feature of the AF observed in experimental models. Using in vivo extracellular recordings, Allesie *et al.* showed that AF induced by programmed electrical stimulation (premature beats or rapid pacing) was characterized by 3-4 wavefronts [5]. In a different experimental model of an explanted sheep heart exposed to acetylcholine, Chen *et al.* [6] found using higher resolution optical mapping that AF is comprised of a larger number of wavelets that are short lived and rarely completely reenter. They also found that when reentry of wavelets did occur, it was generally observed at a fixed location such as the left atrial appendage or the right atrial free wall.

While both electrical and optical mapping have provided significant insight into the dynamics of animal models of AF, they are limited practically since all regions of the atria cannot be accessed or recorded simultaneously.

Computer models offer the advantage of providing information at multiple biological scales and at nearly cellular spatial resolution. Models, however, are limited by the accuracy of the representation of electrophysiological and anatomical details and the computational requirements. Several computer models of electrical propagation in the atria have been recently developed, based on different approaches [7, 8, 9, 10]. Since anatomical structures are known to play a key factor in the development of atrial arrhythmias [11] most of the existing realistic models include structures with different levels of complexity. Anatomical atrial reentry has been simulated in a simplified monolayer model of human atria by Gray *et al.* [7] using the simplified FitzHugh-Nagumo cellular model. Then Harrild and Henriquez developed an anatomically accurate three-dimensional model using an atrial cellular model [8]. However, due to its complexity and increased computational load, this model was used only for simulation of sinus rhythm. A simplified model of canine atria including pectinate muscle structure was proposed recently by Vigmond *et al* [9]. Because of the smaller size compared to human atria, simulations of atrial arrhythmias of one second were performed. These are among the longest simulations of an atrial arrhythmia using a geometrically realistic model.

The combined use of anatomically and electrophysiologically realistic computer models and experimental mapping may help unlock the mechanisms underlying AF. In this paper, we present a new computer model of electrical propagation in the atria with a geometry based on a segmented MRI dataset. In contrast to other anatomically realistic models of the atria, the domain is represented as a three-dimensional surface with obstacles corresponding to the location of major vessels and valves. This model however does not take into account anisotropy. The main advantage of this approach is a significant reduction in computational requirements, enabling the simulation atrial arrhythmias during several seconds (up to 40) in a tissue with realistic size and membrane kinetics. In order to facilitate the link to different mapping modalities, the model outputs both transmembrane potentials and extracellular electrograms.

A key requirement of a computer model of AF is that it produces some number of wavefronts or wavelets that are self sustaining. One source of instability and induction of wavelet breakup is the dependence of the action potential duration (APD) and refractory period on the previous diastolic interval (DI), represented as the restitution curve [12, 13, 14, 15, 16, 17]. While spontaneous breakup has been associated with an increase in the slope of the restitution dependence, AF is usually associated with a loss of rate adaption and general flattening of the restitution dependence [18, 19]. In addition, there is some theoretical evidence that restitution-based breakup may be transient, suggesting that other factors are needed to maintain the arrhythmia [20]. The goal of this study is to investigate the dynamics of restitution-based AF in a model with realistic size and conduction velocity.

In addition we will investigate how electrical remodeling, characterized by a marked reduction of action potential duration without significant change in propagation speed affects the perpetuation of the simulated AF.

2 Methods

2.1 Single Cell Model

The selection of a single cell model is determined by the desired degree of accuracy and the available computer power[21]. Several sophisticated and computationally demanding models based on membrane ionic channel kinetics have been published for sinoatrial cells, atrial cells [22, 18, 23] and ventricular cells. In this study, we have chosen to use the Luo-Rudy model [24], developed originally for ventricular cells. This choice was motivated by the desire to reduce computational load. To approximate the specific properties of atrial cells, the original Luo-Rudy model was modified. The membrane kinetics of the Luo-Rudy model are based on 6 ionic currents (I_{Na} , I_{K_1} , I_{K_p} , I_b , I_K , and I_{si}) involving 6 gating variables and the intracellular calcium concentration. The system dynamics is described by 8 ordinary differential equations, whose numerical integration was performed using a standard approach (Rush-Larsen hybrid scheme [25]). Using previous analyses of the restitution dynamics of the Luo-Rudy model[13, 26, 27, 28], the channel conductances \bar{G}_{Na} , \bar{G}_K and \bar{G}_{si} were adjusted in order to reproduce reasonable atrial action potential duration (APD)[29]. To accomplish this, \bar{G}_{Na} was reduced to 16 mS/cm², \bar{G}_K was set to 0.423 mS/cm² and \bar{G}_{si} to 0.085 mS/cm² as in [28]. The resulting APD, 245 ms, is in agreement with the range of atrial refractory periods in humans (220 to 260 ms [30]). These modifications constitute the baseline model used in the simulations. Any additional modifications will be discussed as they arise. The maximum slow inward conductance, \bar{G}_{si} , is used a control parameter as in [28] to affect the APD and restitution properties. \bar{G}_{si} is varied from 0.085 to 0.05 mS/cm².

2.2 Atrial Geometry

Atrial geometry is known to be a key factor in the development of atrial arrhythmia [11]. Based on the assumptions that atria are thin walled, we have built our anatomic model of the human right and left atrium as three-dimensional monolayer. This approximation has been used in other models of atria [7, 10, 31]. The geometry is based on that obtained from an MRI of the human atria. These MRI data were segmented slice-by-slice and a three-dimensional atrial structure has been reconstructed. This structure has then been processed to create the atrial surface with holes representing the location of veins and the valves. Surface smoothing and some corrections of the contours of veins and valves were necessary. The surface area of

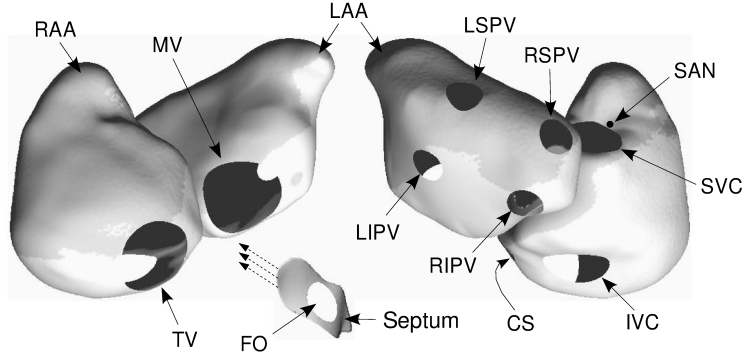


FIGURE 1: Geometry of human atria based on MR images: anterior view (on the left) and posterior view (on the right). The left/right atrium appendages are indicated by LAA/RAA. The major anatomical obstacles are included: tricuspid valve (TV), mitral valve (MV), inferior vena cava (IVC), superior vena cava (SVC), left/right superior pulmonary vein (LSPV/RSPV), left/right inferior pulmonary vein (LIPV/RIPV), and coronary sinus (CS). A cut of the septum is represented with the fossa ovalis (FO). The sino-atrial node (SAN) is represented as a black dot.

both the mitral and tricuspid valves [32] is 4.5 cm^2 , the surface area of the superior and inferior vena cava are 2.8 cm^2 and 3.1 cm^2 , respectively, the surface area of each of the pulmonary veins is 1 cm^2 and the surface area of the coronary sinus is 0.5 cm^2 . The septum has a hole of 1 cm^2 for the fossa ovalis. The entire surface, shown on Fig. 1, has then been meshed using triangular elements.

2.3 Numerical Methods

Electrical propagation in a monodomain cardiac tissue is governed by the partial differential equation [33]

$$C_m \frac{\partial V_m}{\partial t} = S_v^{-1} \nabla \cdot \boldsymbol{\sigma} \nabla V_m + I_{\text{stim}} - I_{\text{ion}} \quad (1)$$

where V_m is the transmembrane potential, $C_m = 1 \text{ } \mu\text{F}/\text{cm}^2$ the membrane capacitance, $S_v = 0.24 \text{ } \mu\text{m}^{-1}$ the cellular surface-to-volume ratio, and $\boldsymbol{\sigma}$ the conductivity tensor. The stimulation current I_{stim} and the ionic current I_{ion} come from the cell model. This equation is solved on the atrial epicardial surface described above. No flux boundary conditions are assumed at the vessels and valves.

Several triangular Delaunay meshes [34] were constructed: a coarse mesh (about 50 000 vertices, 100 000 triangles and an average distance between nearest neighbors of $\langle \Delta x \rangle = 600 \text{ } \mu\text{m}$) for a fast preliminary testing of hy-

potheses, a finer mesh (100 000 vertices, $\langle \Delta x \rangle = 400 \mu\text{m}$) for standard simulations and even finer meshes (200 000 and 400 000 vertices, $\langle \Delta x \rangle = 300 \mu\text{m}$ and $200 \mu\text{m}$) to check the accuracy and ensure the absence of artifacts. With each node i ($i = 1, \dots, N$) located at \mathbf{x}_i is associated a region Ω_i , of area $|\Omega_i|$ (see Fig. 2). The boundary $\partial\Omega_i$ of this region is a union $\partial\Omega_i = \bigcup_k S_{i,k}$ of segments $S_{i,k}$ of length $|S_{i,k}|$ connecting middle points of edges and centers of gravity of triangles (the index k runs over the set of segments defining the contour of the region). This region is composed of several different triangles and is therefore not planar. We also define unit vectors $\mathbf{n}_{i,k}$ which are normal to the segment $S_{i,k}$, tangent to the triangle containing $S_{i,k}$ and outward-oriented with respect to the region Ω_i . The advantages of this approach are that: (1) a true tessellation of the surface is constructed, (2) fluxes have to be estimated in the interior of a triangle and never on an edge, (3) no-flux boundary conditions are correctly and easily taken into account, and (4) non-manifold regions such as surfaces intersection, for instance between the septal wall and the atria, are also integrated into the method.

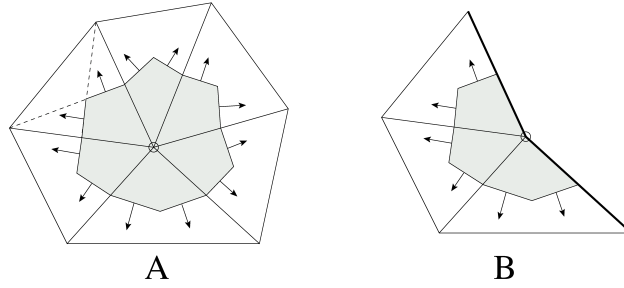


FIGURE 2: Mesh and discretization: region Ω_i associated with a node i (gray polygonal region). (A) Node in the bulk: the polygonal contour of this region successively links middle points of edges and centers of gravity of triangles. Arrows represent outward-oriented normals to segments, weighted by the segment length. (B) Node on the boundary: the region is also well defined in this case and is suitable for a no-flux boundary condition.

The numerical scheme used to solve (1) is based on a finite volume approach [35]. Integrating equation (1) over Ω_i , the following flux conservation equation is obtained:

$$|\Omega_i| C_m \frac{\partial u_i}{\partial t} = S_v^{-1} \sum_k J_{i,k} + |\Omega_i| (I_{\text{stim},i} - I_{\text{ion},i}) \quad (2)$$

where $u_i(t) = V_m(\mathbf{x}_i, t)$, $I_{\text{stim},i}(t) = I_{\text{stim}}(\mathbf{x}_i, t)$ and $I_{\text{ion},i}(t) = I_{\text{ion}}(\mathbf{x}_i, t)$. The current $J_{i,k}$ through the segment $S_{i,k}$ is defined as

$$J_{i,k} = \left(\boldsymbol{\sigma} \nabla V_m(S_{i,k}) \right) \cdot |S_{i,k}| \mathbf{n}_{i,k} \quad (3)$$

where the gradient ∇V_m is assumed constant over each triangle and is computed through linear interpolation in such a way that $J_{i,k}$ becomes a weighted sum of the membrane potentials of neighboring cells. These weights depend on the geometry and on the tissue conductivities, and are computed only once. Using a matrix formulation with $\mathbf{u} = (u_1, \dots, u_N)$, the semi-discretized equation [35] can be written as

$$\frac{\partial \mathbf{u}}{\partial t} = A\mathbf{u} + \mathbf{b}(t) \quad (4)$$

where A is a sparse non-symmetric matrix containing the contribution of all diffusive currents and $\mathbf{b}(t)$ is associated with the ionic currents. The time integration of this equation is performed using an explicit forward Euler scheme with a time step of 20 μs .

In the simulations presented in this paper, the conductivities are homogeneous and isotropic. Inhomogeneities, however, are present in our model due to the anatomical obstacles and the inhomogeneous curvature of the surface. The resistivity of the model for normal propagation is set to $\rho = \sigma^{-1} = 150 \text{ } \Omega \text{ cm}$ for the 100 000 nodes mesh, leading to a conduction velocity of 90 cm/s (mean value over the atria). For the simulation of arrhythmias, the conduction velocity was reduced to 70 cm/s ($\rho = 250 \text{ } \Omega \text{ cm}$). This reduction was performed to decrease wavelength while keeping the conduction velocity within physiological range [36].

As noted earlier, the major objective for this simulation study was to simulate long runs of AF. Trade-offs between model complexity and computational load were necessary. As a result, one second of simulated time requires 1 hour of computation time for a model with 100 000 nodes on a standard PC (Pentium-III 933 MHz). Finer meshes require a smaller time step to ensure numerical stability. The same one-second simulation takes 3 hours for 200 000 nodes. All simulation results presented in this paper were run on a mesh with 100 000 vertices.

2.4 Computing Electrograms and Measures of Organization

To eventually compare data from model simulations with mapping data from animal experiments or human clinical studies, the model was designed to output both transmembrane and extracellular potentials. The extracellular potential ϕ_e is computed using a current source approximation extended to multidimensional tissue [33, 37]. Assuming that the extracellular conductivity is homogeneous and isotropic, ϕ_e is found to be related to the transmembrane current

$$I_m = I_{\text{ion}} - I_{\text{stim}} + C_m \frac{\partial V_m}{\partial t} = S_v^{-1} \nabla \cdot \boldsymbol{\sigma} \nabla V_m \quad (5)$$

through the following equation

$$\phi_e(\mathbf{x}, t) = \frac{1}{4\pi\sigma_e} \int d\mathbf{y} \frac{I_m(\mathbf{y})}{|\mathbf{x} - \mathbf{y}|} \quad (6)$$

where σ_e is the extracellular conductivity.

In a monodomain formulation, I_m is available and allows us to compute the extracellular potential ϕ_e . Since ϕ_e is linearly related to V_m , it is computed for practical reasons as a weighted sum of V_m using the discretized diffusion operator already defined to solve the propagation equation. In the present study, a bipolar electrogram was computed from the difference between the extracellular potential of two points, 2-mm distant from each other and 1 mm from the surface, located in the right atrium free wall.

Membrane potential maps were stored every 5 milliseconds, while electrograms were computed during the simulation every millisecond. In the space plots, action potentials were gray-level-coded, black and white representing respectively 20 and -80 mV. As a measure of complexity and organization, the percentage of excited tissue and the number of wavelets were computed. Cells were considered to be excited when the transmembrane potential exceeded -60 mV. The number of wavelets was defined as the number of connected regions of excited tissue. Non-propagating islands of depolarized tissue were ignored.

3 Results

3.1 Restitution Properties

The restitution dynamics were determined for each \overline{G}_{si} computed on a cable (see Fig. 3). The action potential shape is shown for different cycle lengths in Fig 3A. The baseline model has an APD of 245 ms at rest, and a steep restitution. The effect of the control parameter \overline{G}_{si} on the APD restitution is presented on Fig. 3C. Decreasing values of \overline{G}_{si} correspond to reduced APD and flattened restitution. For values of $\overline{G}_{si} < 0.06$ mS/cm², the maximal slope is smaller than 1. The relationship between steady-state APD and pacing frequency generated by the modified Luo–Rudy model (Fig. 3B) is very similar to that measured experimentally on remodeled atrial cells (see Fig. 1C in [29]). Fig. 3D shows that \overline{G}_{si} has a negligible influence on the conduction velocity which is mainly determined by the sodium current I_{Na} .

3.2 Initiation of Atrial Fibrillation

Wavefronts were initiated by injecting intracellular current in a region located near the sino-atrial (SA) node (see Fig. 1). Several attempts to initiate AF were performed, using the following different stimulation protocols: (1)

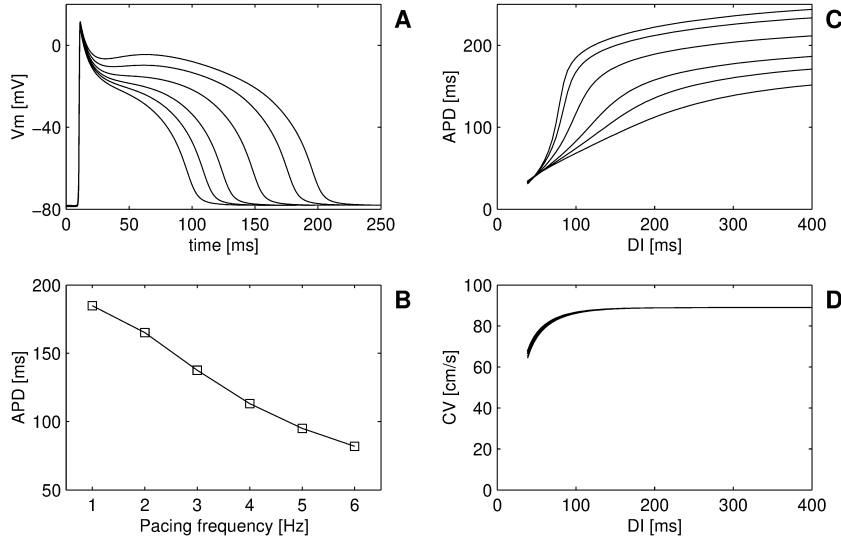


FIGURE 3: Restitution properties measured on a 1.5-cm cable with an element size of $100 \mu\text{m}$ and a resistivity of $200 \Omega \text{ cm}$. Stimulations are delivered to the first cell with a strength of $2 \times$ diastolic threshold. Diastolic intervals (DIs) and action potential durations (APDs) are measured in the middle of the cable using a -60 mV threshold. *Protocol*: A 100-bpm pacing rate is applied until steady-state is reached. Then a S_2 stimulus with different DIs is delivered. *Results*: (A) Action potential shapes (with reduced APD, $\overline{G}_{si} = 0.055 \text{ mS/cm}^2$) are displayed for various cycle lengths from 260 ms to 1000 ms respectively from left to right; (B) Steady-state APD as a function of the pacing frequency ($\overline{G}_{si} = 0.055 \text{ mS/cm}^2$) (C) APD restitution curves of the modified Luo-Rudy model with $\overline{G}_{si} = 0.085, 0.08, 0.07, 0.06, 0.055, 0.05 \text{ mS/cm}^2$ respectively from top to bottom; (D) Corresponding conduction velocity (CV) restitution curves for the same values of \overline{G}_{si} .

S_1 – S_2 protocol, in which a first stimulus delivered to the SA node was followed by an ectopic beat S_2 located within the right atrium near the superior vena cava, 15 mm away from the SA node, (2) S_1 – S_2 – S_3 protocol with an additional S_3 ectopic beat at the same location as the S_2 in (1), and (3) burst pacing protocol consisting of a 20-Hz (or 25-Hz) stimulation applied at the SA node during several seconds. All stimuli were delivered to a 3-mm^2 area with a strength of $80 \mu\text{A/cm}^2$. Due to the refractoriness of the action potentials, most of the stimuli applied during rapid pacing fail to elicit a response and generate a propagating wavefront. As a result, the burst pacing protocol is equivalent to a sequence of premature stimuli. Its major advantage, however, is that it does not require any adjustment of timing or location of ectopic beats, which can be a time-consuming task due to the high sensitivity of the system to these parameters. Moreover, the pacing frequency is not critical; burst-pacing protocols at 20 or 25 Hz lead to very similar results.

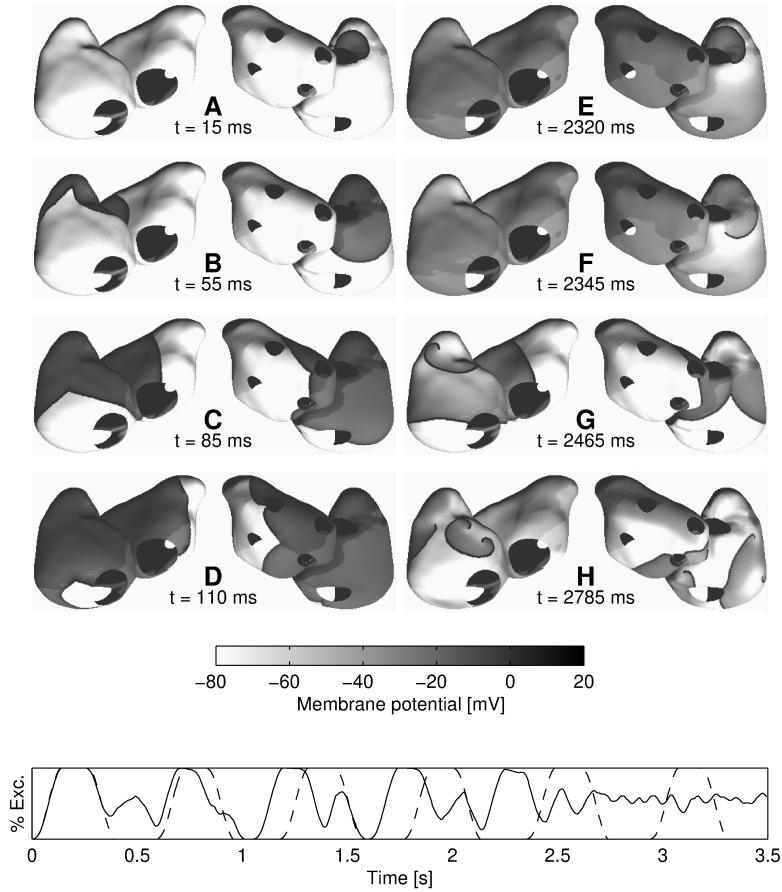


FIGURE 4: Initiation of AF in a model with $\overline{G}_{si} = 0.08$ mS/cm² using a 20-Hz burst-pacing stimulation protocol applied at the SA node during 3.5 s (run on the 100 000-nodes mesh). The bottom panel displays the percentage of excited tissue (% Exc) during the initiation phase (continuous line) as well as during sinus rhythm at 100 bpm with the same tissue properties (dashed line). These space plots were all stored during burst-pacing. Thick black lines represent wavefronts. (A)–(D) First beat showing normal activation with a conduction velocity of 70 cm/s. (E) Initiation of AF after the 3rd propagating beat generated by the stimulation protocol), (F) 4th propagating beat, (G) 7th propagating beat, (H) 9th propagating beat.

Fig. 4 illustrates the 20-Hz burst pacing protocol in our atrial model with $\overline{G}_{si} = 0.08$ mS/cm². Fig. 4A–D show the first beat (equivalent to a sinus beat), which propagates from the right to the left atrial tissue. Atrial activation terminates in the left lateral wall below the appendage, where the three wavefronts converge. Despite some differences due to the use of a simplified geometry, the global behavior of the activation maps is comparable to the ones from experimental data [30] or other anatomical models [8]. Figs.

4E–H show how after several beats, burst pacing degenerates into multiple wavelets, heretofore referred to as simulated AF (SAF). SAF was observed as several independent wavelets traveling randomly in the tissue without external stimulation.

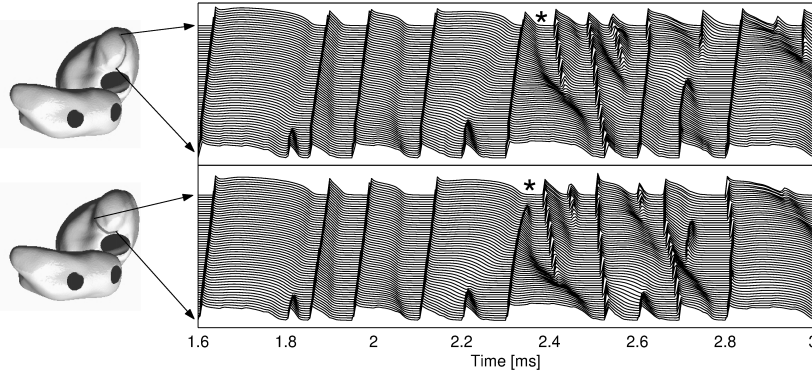


FIGURE 5: Illustration of the mechanism of conduction block occurring in the right atrium appendage. The membrane potentials along two lines from the sino-atrial node towards the appendage are plotted. The star (\star) indicates the conduction block arising along the second line (bottom panel) and not along the first one (top panel).

To better understand the mechanism leading to SAF in our homogeneous model, we plotted the evolution of membrane potentials along two lines from the sino-atrial node towards the right atrium appendage. Fig. 5 shows a conduction block arising along only one of the two paths, a phenomenon made possible by the symmetry breaking due to the non-planar geometry. The first wavebreak is therefore obtained through a mechanism of non-uniform alternans [38] due to both restitution and geometry. Interactions with the next wavelets initiated at sino-atrial node by the stimulation protocol and with boundaries [39] lead to SAF.

As noted earlier, the model can output both transmembrane and extracellular potentials. Fig. 6 shows the simulated electrogram and corresponding transmembrane potential for a cell located in the right atrium free wall. As shown in Fig. 6A, the regular shape of baseline electrogram for the first three beats of burst pacing is similar that recorded experimentally during sinus rhythm. Figs. 6B–C show that the morphology of the electrograms changes markedly during SAF. The electrograms are characterized by both positive and negative complexes as well as single and multi-phasic potentials. Such complex electrogram morphology have been reported in animal mapping studies of AF [40].

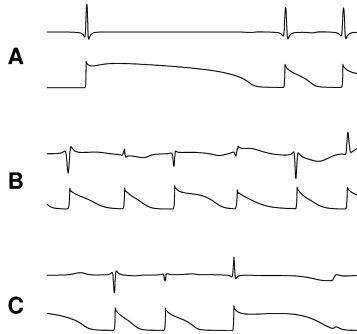


FIGURE 6: Examples of bipolar electrograms with the corresponding transmembrane potential computed at the same location in the right atrium free wall using a 20-Hz burst-pacing stimulation protocol applied at the SA node during 3.5 s. The time window is 0.5 s wide. (A) The 3 first beats initiated by the stimulation protocol. (B)–(C) examples of bipolar electrograms during AF at time $t = 5.5$ s and $t = 6.8$ s respectively.

3.3 Unsustained Atrial Fibrillation

Using the baseline model, none of the atrial arrhythmia initiation protocols (S_1 – S_2 , S_1 – S_2 – S_3 or burst pacing) succeeded in producing sustained SAF. Most of the simulated arrhythmias were unstable and tended to terminate through mutual interactions of wavefronts or interactions with boundary and refractory tissue. The average SAF duration was approximately 4–5 seconds. This antifibrillatory property in the baseline conditions with longer duration action potentials is similar to that observed on the normal human atria, where most AF episodes convert to sinus rhythm after a few seconds [5].

Fig. 7 shows an example of the initiation of unsustained AF in the baseline model with a 20-Hz burst pacing protocol applied during 3.5 seconds. This figure displays the activation potential maps, and both the electrogram and transmembrane potential for an atrial cell located in the right atrium free wall.

Fig. 6B and 6C show a zoom of the action potential and electrogram at time $t = 5.5$ s and $t = 6.8$ s respectively. Simultaneously, two measures of the degree of organization, namely the percentage of excited tissue and number of wavelets, are displayed. A reference value for the percentage of excited tissue during sinus rhythm is presented in Fig. 4. In this example, SAF is sustained for 8.4 seconds and is terminated by a gradual reorganization and a reduction of the number of wavelets and finally by the collision of three wavefronts (see Fig. 7H). During SAF, the activity oscillates between periods of complex cardiac activity and periods with reduced activity. This slowed activity (at time $t \approx 4.5$ s, $t \approx 6.5$ s and $t \approx 8.5$ s) is characterized by

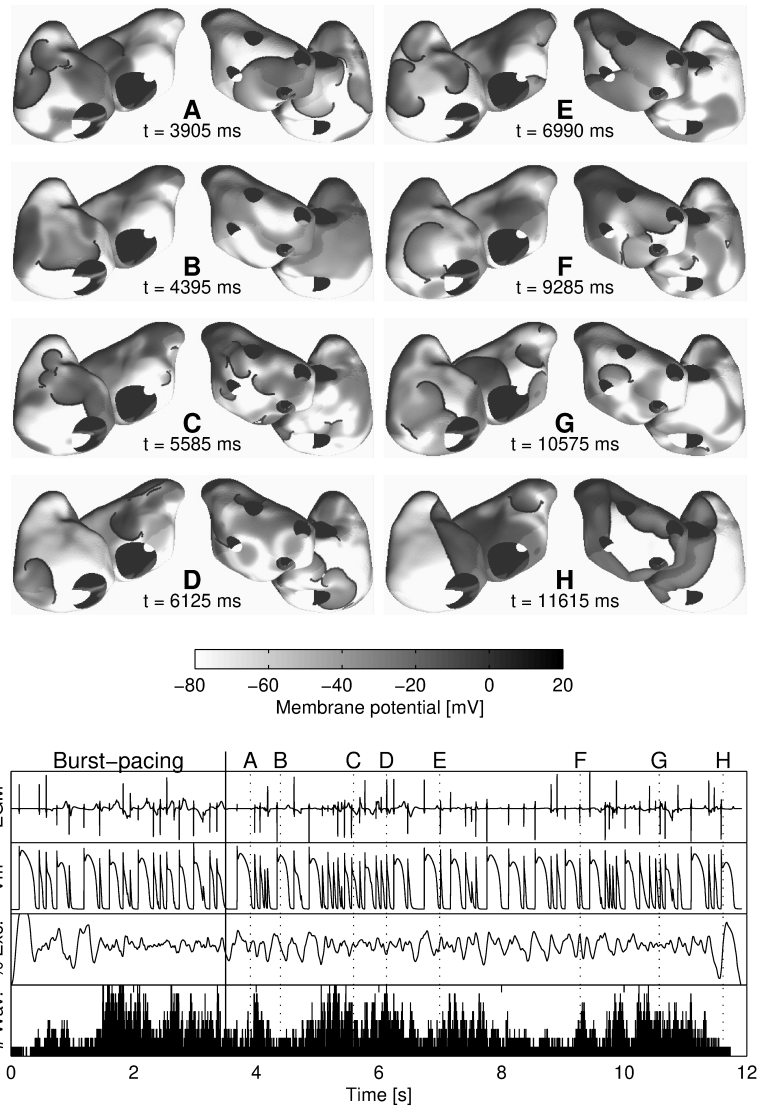


FIGURE 7: Example of unsustained fibrillation on the baseline model ($\overline{G}_{si} = 0.085$ mS/cm²) using a 20-Hz burst-pacing stimulation protocol applied at the SA node during 3.5 s (run on the 100000-nodes mesh). The four bottom graphs display the evolution of the bipolar electrogram (EGM), the action potential (V_m), both recorded at the same location in the right atrium free wall, the percentage of excited tissue (% Exc) and the number of wavelets (# Wav). (A)–(G) Space plots of membrane potentials during AF showing several interacting wavelets. Thick black lines represent wavefronts. (H) Self-termination after 8.4 s of AF.

a decreased rate, larger and slower variations of the percentage of excited tissue, and by a small number of wavelets (1 to 3). These situations are

similar to those observed near the self-termination of AF. Consequently, a slight perturbation will affect the duration in the SAF.

SAF duration, measured as the time between the last burst pacing beat and the repolarization of the whole tissue, was computed for different initial states of tissue just after the end of the stimulation protocol. Table 1 summarizes the results, and includes the two measures of the degree of organization: the percentage of excited tissue and the number of wavelets. The data illustrates the difficulty in predicting the duration of SAF from either the initial state of the tissue or the number of wavelets. No obvious correlation has been found between these measures of degree of organization and


Initial State	Time	% Excited Tissue	Number of Wavelets	AF Duration
	1500 ms	60 %	7	2.5 s
	2000 ms	57 %	3	1.1 s
	2500 ms	59 %	5	1.1 s
	3000 ms	55 %	4	3.5 s
	3500 ms	44 %	1	8.4 s
	4000 ms	49 %	4	7.8 s
	4500 ms	58 %	2	4.3 s
	5000 ms	49 %	5	2.7 s

TABLE 1: Relations between the initial state and AF duration. “Time” refers to the duration of the stimulation protocol. On the space plots, refractory tissue is colored in dark gray. Black lines represent wave fronts.

duration of AF, although very short runs of SAF can usually be identified. These results suggest that other indices of complexity or organization are needed.

3.4 Remodeling and Sustained Atrial Fibrillation

Significantly longer runs of SAF could be obtained by an abrupt reduction of the APD. Such changes in APD are often seen experimentally and clinically after many seconds of atrial fibrillation [19]. In this study, the initiation phase was separated from the perpetuation phase. SAF was induced by applying a burst pacing protocol on the baseline model. After some predefined period, the value of the control parameter \overline{G}_{si} was instantaneously reduced to produce shorter APDs and a flatter restitution (Fig. 3). In order to see the effect of remodeling on duration of SAF, the same baseline model is used for the initiation phases of Figs. 7 and 9, but abrupt remodeling is applied in the example of Fig. 9 after 3.5 s (\overline{G}_{si} was reduced from 0.085 to 0.07 mS/cm²). The effect of APD shortening is a prolongation of the duration of SAF, which is sustained for more than 24 seconds. As the APD reduces, the mean number of wavelets increases due to the decrease in wavelength (see Fig. 8). We can also observe that the rate of SAF is increased for reduced values of \overline{G}_{si} .

3.5 Effect of Action Potential Duration Restitution

Wavebreak has been shown to be facilitated when using action potential dynamics with a steep restitution curve (*i.e.* slope greater than 1) [12, 13].

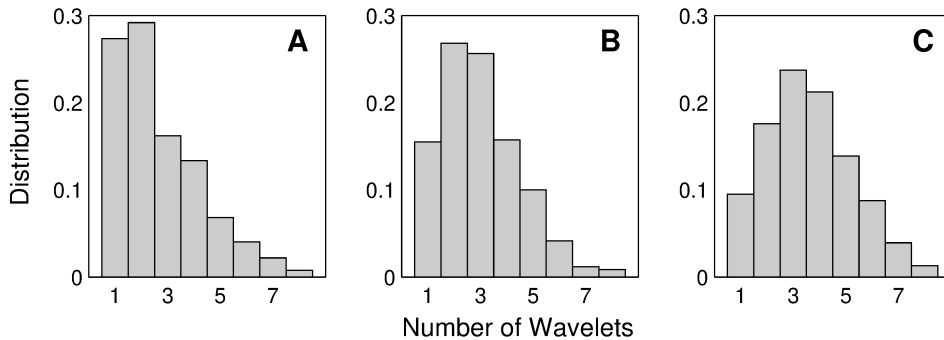


FIGURE 8: Distribution of the number of wavelets during AF initiated by a 20-Hz burst pacing at SA node during 3.5 s on the baseline model. (A) Without remodeling ($\overline{G}_{si} = 0.085$ mS/cm²), leading to an unsustained AF of duration 8.4 s and with an average number of wavelets $\langle w \rangle = 2.7$. (B) After remodeling ($\overline{G}_{si} = 0.07$ mS/cm²), leading to sustained AF with $\langle w \rangle = 3.0$. (C) after remodeling ($\overline{G}_{si} = 0.05$ mS/cm²), leading to sustained AF with $\langle w \rangle = 3.6$.

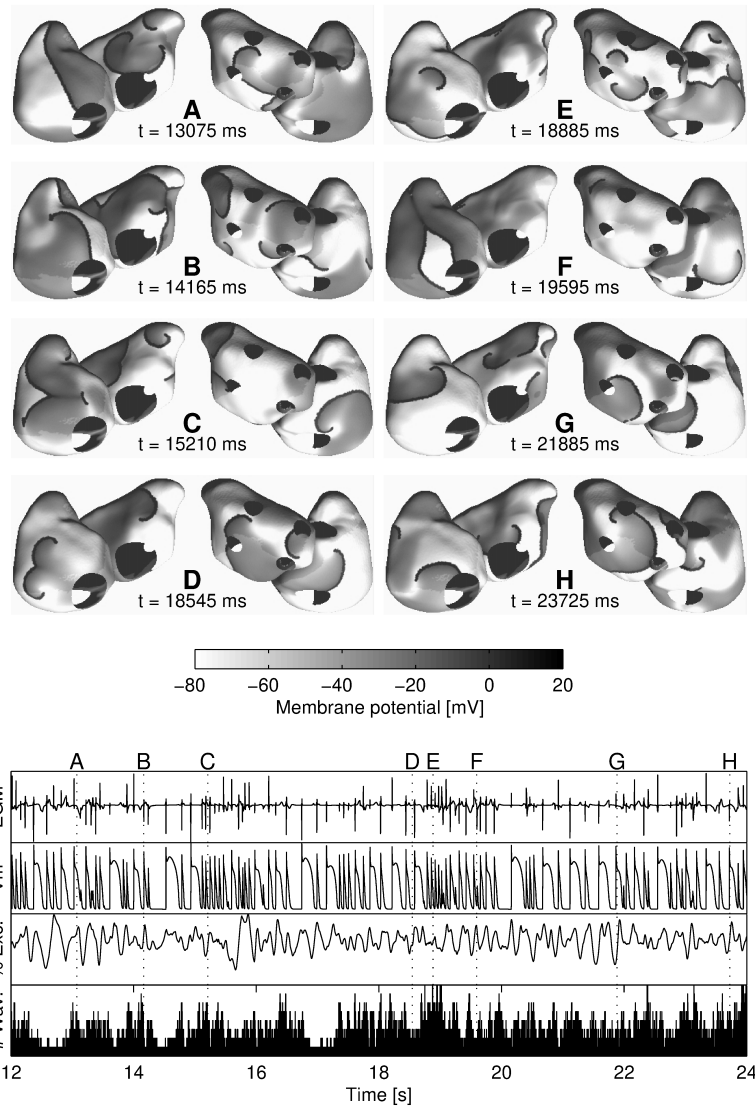


FIGURE 9: Example of sustained fibrillation obtained after an abrupt remodeling (run on the 100 000-nodes mesh). A 20-Hz burst-pacing stimulation protocol was applied at the SA node during 3.5 s on the baseline model (exactly as in Fig.7) followed by an abrupt remodeling at time $t = 3.5$ s where the conductance \bar{G}_{si} was instantaneously set to 0.07 mS/cm² (instead of 0.085 mS/cm² in the baseline model). The four bottom graphs display the evolution of the bipolar electrogram (EGM), the action potential (V_m), both recorded at the same location in the right atrium free wall, the percentage of excited tissue (% Exc) and the number of wavelets (# Wav). (A)–(H) Space plots of membrane potentials during sustained AF. Thick black lines represent wavefronts.

Thus, the impact of the restitution dynamics of the action potential on the initiation and perpetuation of SAF was investigated. To quantify the

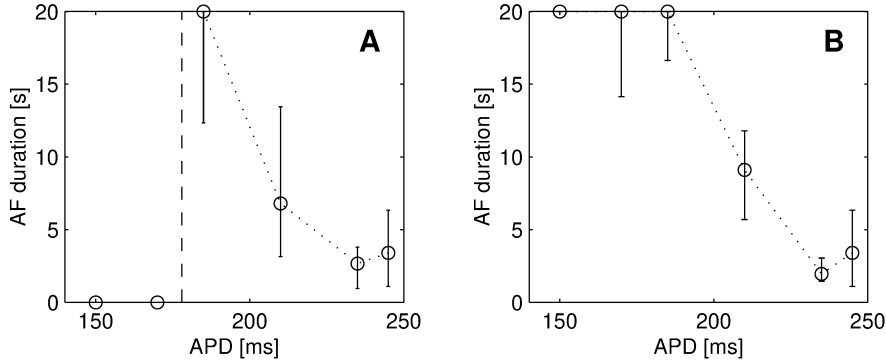


FIGURE 10: Average duration of AF as a function of the control parameter \overline{G}_{si} . A duration >20 s was considered as sustained AF. The circles represent the median of AF durations distribution, and the error bars are associated with the first and third quartile. For this illustration, \overline{G}_{si} was replaced by its associated APD (conversion table: an APD of 245, 235, 210, 185, 170, 150 ms is associated with a \overline{G}_{si} of 0.085, 0.08, 0.07, 0.06, 0.055, 0.05 mS/cm² respectively). (A) AF durations (without remodeling). The vertical dashed line gives the value for which the maximal slope of the corresponding APD restitution curve is 1. Zero AF duration means that AF could not be initiated. (B) AF durations after remodeling. The APD shown in the x-axis is the APD after remodeling.

effect of APD restitution, the same initiation protocol was used on models with decreasing value of the control parameter \overline{G}_{si} . We successively used $\overline{G}_{si} = 0.085$ (baseline model), 0.08, 0.07, 0.06, 0.055 and 0.05 mS/cm², with all other parameter values remaining the same as in the baseline model. The resulting flattening of restitution curve is obtained in combination with reduced APD (see Fig. 3). For each value of \overline{G}_{si} , 15 burst-pacing protocols with different durations (from 1.5 to 5 s) were applied without remodeling, and SAF duration was measured. If the SAF duration was at least 20 s, SAF was classified as sustained and the simulation was terminated. Fig. 10A displays the median, the first and third quartiles of the resulting distributions of SAF duration. As explained above, when the slope of the APD restitution function is always smaller than 1 (APD = 150 and 170 ms on Fig. 10A), initiation of AF was usually not possible. Although the initiation of AF was more difficult with a slope close to 1, the resulting SAF lasted longer because the APD, and thus the wavelength, was shortened.

To investigate the effect of remodeling on SAF duration, the same set of experiments (with remodeling) was repeated for 8 different burst pacing initiation protocols, all applied on the baseline model, and for 5 different reduced values of \overline{G}_{si} (remodeling), namely 0.08, 0.07, 0.06, 0.055 and 0.05 mS/cm². Fig. 10B summarizes the results. In these simulations, SAF is initiated directly in the remodeled tissue. Remodeling decreases the

wavelength, hence prolonging the duration of SAF. Moreover, sustained AF was observed even for values of \overline{G}_{si} for which SAF could not be initiated. The reason for this anomalous behavior is that despite the flat static restitution for this \overline{G}_{si} , wavebreaks can still occur because the dynamical APD restitution has a slope slightly greater than 1 for short DIs. Fig. 11 shows the dynamical restitution curve measured during SAF with a remodeled \overline{G}_{si} value of 0.055 mS/cm². This curve is influenced by all the local changes in gradients of APD due to collisions and interactions with boundaries during SAF.

4 Concluding Remarks

We have presented a computationally efficient computer model of human atria with a geometry derived from a MRI dataset of the human heart. It combines the advantage of being able to simulate one second of arrhythmia in one hour on a single processor with a good representation of the atrial surface and its main anatomical obstacles. Such an approach may eventually lead to the creation of patient specific model to test various therapies.

In our baseline model with normal conduction velocity and action potential duration, SAF could be induced using a single-site burst pacing protocol

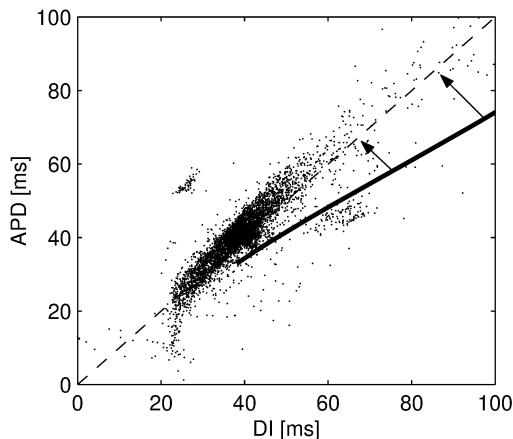


FIGURE 11: Dynamical APD restitution curve during AF after remodeling in a model with $\overline{G}_{si} = 0.055$ mS/cm² together with the corresponding static restitution curve (plain line). The dashed diagonal line has a slope 1. Both arrows emphasize the dynamical steepening of the restitution during AF. APDs and DIs are measured with a -60 mV threshold and computed over 100 cells located on the epicardial surface. Very short APDs and DIs (< 30 ms) are mainly due to electrotonic effects produced by wavefront-waveback collisions and cannot be considered as action potentials. The presence and the value of extremely low APD and DI strongly depends on the thresholding method used to compute them.

despite the uniform membrane and tissue properties. In this case, the initiator is restitution-based. The first wavebreaks tend to occur in regions where the curvature varies rapidly (right and left appendages for example). Note that without the non-uniform curvature, the single site stimulation protocol would not produce the required wavebreak. We have shown that atrial geometry is a factor that can create functional heterogeneities (Fig. 5). The subsequent creation of multiple wavebreaks is due primarily to the restitution dynamics (see Fig. 3). For a slope of restitution curve greater than one, SAF is inducible. On the other hand, if the slope is smaller than one, burst-pacing could not induce SAF in this model with uniform membrane and conduction properties. In this case, other mechanisms of heterogeneities have to be involved for initiation.

In most of the cases of SAF, the number of wavelets on the surface varies between 1 and 7. This is consistent with the number observed in experimental models of AF [5, 30]. Although SAF was inducible, it was not sustained using the baseline model. Rather SAF converted to sinus rhythm after a few seconds, usually preceded by a gradual reorganization and decrease in the number of wavelets. The self-termination could be explained by the wide range of APDs (from 40 to 245 ms) and by the fact that large values of APD can create large areas of refractory tissue, leading to a reduction in the number of wavelets and hence self-termination. Thus, the simulations suggest that restitution-based breakup in an isotropic model with realistic size and conduction velocity is transient. While not tested, increasing the size or adding anisotropy to reduce wavespeed in some directions may prolong the SAF. The simulations also showed that the time to self-termination was difficult to predict from potential maps or from indices of organization such as the number of wavelets. More sophisticated measures of organization need to be developed.

Sustained SAF was observed only after a reduction in APD. Such electrical remodeling is often seen in patients with paroxysmal AF. The significantly longer durations of SAF was obtained even when the cells had apparently flat restitution curves. Therefore while initiation of wavebreak and SAF in our model required a restitution curve with a slope greater than 1, perpetuation did not. It is important to note, however, that the simulations show that even if the static restitution curve has a slope smaller than one, the dynamical restitution curve can be much steeper if short APDs are possible. The larger range of APD (particularly for short DIs) during SAF is likely due to the effects of boundaries and collisions. The difference between the dynamical and static restitution in a domain with complex geometry may explain how AF can be maintained in uniform tissues that appear to have a reduction in rate dependence (e.g. the acetylcholine model of AF). The number of wavelets during AF is also dependent on APD. For shorter APDs, the average number of wavelets is increased since wavelength is decreased.

Acknowledgments

This study was made possible by grants from the Theo-Rossi-Di-Montelera Foundation, Medtronic Europe, the Swiss Governmental Commission of Innovative Technologies (CTI) and the Swiss National Science Foundation (SNSF). The authors wish to thank Ryan Lahm, Drs. Josée Morissette and Arthur Stillman who kindly furnished the atrial geometry surface model.

References

- [1] M. A. Allesie, W. Lammers, F. Bonke, and J. Hollen, “Experimental evaluation of Moe’s multiple wavelet hypothesis of atrial fibrillation,” in *Cardiac Arrhythmias* (D. Zipes and J. Jalife, eds.), pp. 265–276, Grune & Stratton, New York, 1985.
- [2] M. A. Allesie, P. Rensma, J. Brugada, J. Smeets, O. Penn, and C. Kirchhof, “Pathophysiology of atrial fibrillation,” in *Cardiac Electrophysiology: From Cell to Bedside* (D. Zipes and J. Jalife, eds.), pp. 548–559, W.B. Saunders Company, Philadelphia, 1990.
- [3] H. Sih, D. Zipes, E. Berbari, and J. Olgin, “A high-temporal resolution algorithm for quantifying organization during atrial fibrillation,” *IEEE Trans. Biomedical Eng.*, vol. 46, no. 4, pp. 440–450, 1999.
- [4] M. Mansour, R. Mandapati, O. Berenfeld, J. Chen, F. Samie, and J. Jalife, “Left-to-right gradient of atrial frequencies during acute atrial fibrillation in the isolated sheep heart,” *Circ.*, vol. 103, pp. 2631–2636, 2001.
- [5] M. A. Allesie, P. L. Rensma, and J. Brugada, “Pathophysiology of atrial fibrillation,” in *Cardiac Electrophysiology: From Cell to Bedside* (D. P. Zipes and J. Jalife, eds.), pp. 548–559, W. B. Saunders, Philadelphia, 1995.
- [6] J. Chen, R. Mandapati, O. Berenfeld, A. C. Skanes, R. A. Gray, and J. Jalife, “Dynamics of wavelets and their role in atrial fibrillation in the isolated sheep heart,” *Cardiovasc. Res.*, vol. 48, pp. 220–232, 2000.
- [7] R. A. Gray and J. Jalife, “Ventricular fibrillation and atrial fibrillation are two different beasts,” *Chaos*, vol. 8, pp. 65–78, Mar. 1998.
- [8] D. M. Harrild and C. S. Henriquez, “A computer model of normal conduction in the human atria,” *Circ. Res.*, vol. 87, pp. e25–e36, 2000.
- [9] E. J. Vigmond, R. Ruckdeschel, and N. Trayanova, “Reentry in a morphologically realistic atrial model,” *J. Card. Electr.*, vol. 12, pp. 1046–1054, Sept. 2001.

- [10] C. Zemlin, H. Herzel, S. Ho, and A. Panfilov, “A realistic and efficient model of excitation propagation in the human atria,” in *Computer Simulation and Experimental Assessment of Cardiac Electrophysiology* (N. Virag, O. Blanc, and L. Kappenberger, eds.), pp. 29–34, Futura Publishing, Armonk, NY, 2001.
- [11] R. A. Gray, K. Takkellapati, and J. Jalife, “Dynamics and anatomical correlates of atrial flutter and fibrillation,” in *Cardiac Electrophysiology: From Cell to Bedside* (D. P. Zipes and J. Jalife, eds.), pp. 346–365, W. B. Saunders, Philadelphia, 1995.
- [12] A. Vinet, D. R. Chialvo, D. C. Michaels, and J. Jalife, “Nonlinear dynamics of rate-dependent activation in models of single cardiac cells,” *Circ. Res.*, vol. 67, no. 6, pp. 1510–1524, 1990.
- [13] Z. Qu, A. Garfinkel, P.-S. Chen, and J. N. Weiss, “Mechanisms of discordant alternans and induction of reentry in simulated cardiac tissue,” *Circ.*, vol. 102, pp. 1664–1670, Oct. 2000.
- [14] M.-H. Lee, Z. Qu, G. Fishbein, S. Lamp, E. Chang, T. Ohara, O. Voroshilovsky, J. Kil, A. Hamzei, N. Wang, S.-F. Lin, J. N. Weiss, A. Garfinkel, H. Karagueuzian, and P.-S. Chen, “Patterns of wave break during ventricular fibrillation in isolated swine right ventricle,” *Am. J. Physiol. Heart Circ. Physiol.*, vol. 281, pp. H253–H265, 2001.
- [15] H. Karagueuzian and B. Kogan, “Action potential duration restitution dynamics and its relation to spiral wave formation: an experimental and computer simulation study,” in *Cardiac Mapping* (M. B. M. Shenasa and G. Breithardt, eds.), pp. 627–645, Futura Publishing, Mt. Kisco, New York, 1993.
- [16] R. G. Jr., M. Watanabe, and N. Otani, “Restitution properties and dynamics of reentry,” in *Cardiac Electrophysiology: From Cell to Bedside, 3rd Edition* (D. Zipes and J. Jalife, eds.), pp. 378–385, W.B. Saunders Company, Philadelphia, 2000.
- [17] T. Ohara, K. Ohara, J.-M. Cao, M.-H. Lee, M. Fishbein, W. Mandel, P.-S. Chen, and H. Karagueuzian, “Increased wave break during ventricular fibrillation in the epicardial border zone of hearts with healed myocardial infarction,” *Circ.*, vol. 103, pp. 1465–1472, 2001.
- [18] M. Courtemanche, R. J. Ramirez, and S. Nattel, “Ionic targets for drug therapy and atrial fibrillation-induced electrical remodeling: Insights from a mathematical model,” *Card. Res.*, vol. 42, pp. 477–489, 1999.
- [19] S. Nattel and D. Li, “Ionic remodeling in the heart: Pathophysiological significance and new therapeutic opportunities for atrial fibrillation,” *Circ. Res.*, vol. 87, pp. 440–447, 2000.

- [20] M. Courtemanche, “Complex spiral wave dynamics in a spatially distributed ionic model of cardiac electrical activity,” *Chaos*, vol. 6, no. 4, pp. 579–600, 1996.
- [21] E. Cherry, H. Greenside, and C. Henriquez, “A space–time adaptive method for simulating complex cardiac dynamics,” *Physiol. Rev. Lett.*, vol. 84, pp. 1343–1348, 2000.
- [22] M. Courtemanche, R. J. Ramirez, and S. Nattel, “Ionic mechanisms underlying human atrial action potential properties: Insights from a mathematical model,” *Am. J. Physiol.*, vol. 275, pp. H301–H321, 1998.
- [23] A. Nygren, C. Fiset, L. Firek, J. W. Clark, D. S. Lindblad, R. B. Clark, and W. R. Giles, “Mathematical model of an adult human atrial cell. the role of K^+ currents in repolarization,” *Circ. Res.*, vol. 82, pp. 63–81, 1998.
- [24] C.-H. Luo and Y. Rudy, “A model of the ventricular cardiac action potential,” *Circ. Res.*, vol. 68, pp. 1501–1526, June 1991.
- [25] S. Rush and H. Larsen, “A practical algorithm for solving dynamic membrane equations,” *IEEE Trans. Biomed. Eng.*, vol. 25, pp. 389–392, July 1978.
- [26] Z. Qu, J. Kil, F. Xie, A. Garfinkel, and J. N. Weiss, “Scroll waves dynamics in a tree-dimensional cardiac tissue model: Roles of restitution, thickness and fiber orientation,” *Biophys. J.*, vol. 78, pp. 2761–2775, June 2000.
- [27] J. N. Weiss, A. Garfinkel, H. S. Karagueuzian, Z. Qu, and P.-S. Chen, “Chaos and the transition to ventricular fibrillation. a new approach to antiarrhythmic drug evaluation,” *Circ.*, vol. 99, pp. 2819–2826, 1999.
- [28] Z. Qu, J. N. Weiss, and A. Garfinkel, “From local to global spatiotemporal chaos in a cardiac tissue model,” *Phys. Rev. E*, vol. 61, pp. 727–732, Jan. 2000.
- [29] D. Li, L. Zhang, J. Kneller, and S. Nattel, “Potential ionic mechanism for repolarization differences between canine right and left atrium,” *Circ. Res.*, vol. 88, pp. 1168–1175, 2001.
- [30] J. L. Cox, T. E. Canavan, and R. B. Schuessler, “The surgical treatment of atrial fibrillation. II. Intraoperative electrophysiologic mapping and description of the electrophysiologic basis of atrial flutter and atrial fibrillation,” *J. Thorac. Surg.*, vol. 101, pp. 406–426, 1991.
- [31] O. Blanc, N. Virag, J.-M. Vesin, and L. Kappenberger, “A computer model of human atria with reasonable computation load and realistic

- anatomical properties,” *IEEE Trans. Biomed. Eng.*, vol. 48, pp. 1229–1237, Nov. 2001.
- [32] E. Braunwald, “Valvular heart diseases,” in *Heart Diseases, a Textbook of Cardiovascular Medicine* (E. Braunwald, ed.), pp. 1007–1077, W. B. Saunders, Philadelphia, 1992.
- [33] R. Plonsey and R. C. Barr, *Bioelectricity: A Quantitative Approach*. New York: Kluwer Academic / Plenum Publishers, second ed., 2000.
- [34] P. L. George and H. Borouchaki, *Delaunay triangulation and meshing: application to finite elements*. Paris: Hermes, 1998.
- [35] R. S. Varga, *Matrix Iterative Analysis, 2nd edition*. Berlin: Springer, 2000.
- [36] R. J. Schilling, A. H. Kadish, and N. S. Peters, “Endocardial mapping of atrial fibrillation in the human right atrium using a non-contact catheter,” *Eur. Heart J.*, vol. 21, pp. 550–564, 2000.
- [37] A. van Oosterom, “Forward and inverse problems in electrocardiography,” in *Computational Biology of the Heart* (A. Panfilov and A. Holden, eds.), pp. 295–343, , John Wiley & Sons, Chichester, 1997.
- [38] J. J. Fox, M. L. Riccio, F. Hua, E. Bodenschatz, and R. F. Gilmour Jr, “Spatiotemporal transition to conduction block in canine ventricle,” *Circ. Res.*, vol. 90, pp. 289–296, 2002.
- [39] C. Cabo, A. M. Pertsov, J. M. Davidenko, W. T. Baxter, R. A. Gray, and J. Jalife, “Vortex shedding as a precursor of turbulent electrical activity in cardiac muscle,” vol. 70, pp. 1105–1111, Mar. 1996.
- [40] N. M. S. De Groot and M. Allesie, “Ten years of mapping of human atrial fibrillation,” in *Computer Simulation and Experimental Assessment of Cardiac Electrophysiology* (N. Virag, O. Blanc, and L. Kappenberger, eds.), pp. 3–11, Futura Publishing, Armonk, NY, 2001.